DOI:10.1109/TOH.2014.2371025

Analysis of Operational Comfort in Manual Tasks Using Human Force Manipulability Measure

Yoshiyuki Tanaka, *Member, IEEE*, Kazuo Nishikawa, Naoki Yamada, and Toshio Tsuji, *Member, IEEE*

Abstract—This paper proposes a scheme for human force manipulability (HFM) based on the use of isometric joint torque properties to simulate the spatial characteristics of human operation forces at an end-point of a limb with feasible magnitudes for a specified limb posture. This is also applied to the evaluation/prediction of operational comfort (OC) when manually operating a human-machine interface. The effectiveness of HFM is investigated through two experiments and computer simulations of humans generating forces by using their upper extremities. Operation force generation with maximum isometric effort can be roughly estimated with an HFM measure computed from information on the arm posture during a maintained posture. The layout of a human-machine interface is then discussed based on the results of operational experiments using an electric gear-shifting system originally developed for robotic devices. The results indicate a strong relationship between the spatial characteristics of the HFM and OC levels when shifting, and the OC is predicted by using a multiple regression model with HFM measures.

Index Terms—Human-machine interface, human-centered design, human force manipulability, operational comfort

1 Introduction

Within a vehicle cockpit, driving interfaces such as the shift lever, steering wheel, and gas pedal may not be arranged in the best positions for the driver because of the difficulty of designing the layout in a limited space while considering human operational comfort (OC) in the early stages of vehicle development. The human-centered design of an interface arrangement remains a major issue, especially in the automobile industry. It would be easier to produce a more comfortable interior package if a human-centered layout that takes human factors into account could be generated successfully.

Y. Tanaka is with Graduate School of Engineering, Nagasaki University, 1-14 Bunkyou-machi, Nagasaki 852-8521, Japan (e-mail: ytnk@nagasaki-u.ac.jp).
K. Nishikawa and N. Yamada with Mazda Motor Corporation, 3-1 Shinchi, Fuchu-cho, Aki-gun, Hiroshima 730-8670, Japan (nishikawa.ka@mazda.co.jp, yamada.na@mazda.co.jp).
T. Tsuji is with Graduate of Engineering, Hiroshima University, 1-4-1 Kagamiyama, Higashi-hiroshima 739-8527, Japan (tsuji@bsys.hiroshima-u.ac.jp).

To date, ergonomic studies of posture comfort/discomfort, with/without physical loads, have been conducted mainly for reducing workload and avoiding work-related musculoskeletal disorders resulting from repetitive factory jobs [1], [2], [3], [4]. For example, Kee and Lee [4] determined the presence of stress in joints at certain joint angles and under the influence of certain motions in the sitting and standing postures by analyzing the perceived discomfort recorded in an experiment and then proposed a ranking system for evaluating the load on a stressed joint based on the measured data. Based on such ergonomic data, a few ergonomic computer aided design (CAD) tools such as RAMSIS and TRANSAM-JACK have been developed to reduce the duration and cost of product development. Such ergonomic CAD tools display human figures (mannequins) along with kinematic analyses of vision, posture, and motion-effort for a target operation. They help with the process of interactive product design and are widely used in the automobile industry. However, the OC level of a driving interface cannot be determined and implemented in practice owing to the lack of general evidence for evaluating subjective feelings experienced when performing operations.

On the other hand, the mechanical performance of robotic manipulators with multi-joint mechanisms is often analyzed based on the robot manipulability as derived from the kinematic and dynamic formulae describing the relationship between the joints and the endpoint relative to the inertia [5], velocity and force [6], [7], and acceleration [8]. This method is used to evaluate a robot's performance at an endpoint, such as its ability to generate force, based on its link configurations. Some studies have applied this robotic technique to the analysis of human hand movements [9], the mechanical design of artificial limbs [10], and the development of automobile interfaces [11]. Conventional robot manipulability, however, does not consider biological motor properties such as the feasible magnitude of joint torque, which should be

considered for human performance analysis as well as for the human-centered design of human-machine interfaces.

Many fundamental studies have been conducted to investigate the joint torque-angle relationship in the upper limb [12], [13], [14], lower limb [15], [16], and in both limbs [17], [18]. However, these studies on human joint torque have not addressed the relationship with force production by an endpoint or the quantitative evaluation of human force-generation performance in task spaces.

In the present study, a new manipulability measure using human joint torque characteristics, called human force manipulability (HFM), is proposed to estimate the feasible magnitude of human-generated force at an endpoint in an arbitrary direction for a certain limb posture. We then demonstrate that the OC of an interface device can be evaluated/predicted using a multiple regression model with the proposed HFM measure through, for example, a set of laboratory experiments involving a gear-shifting operation by the arm.

The remainder of this paper is organized as follows: Section **2** describes the formulation of the HFM measure after first outlining robot force manipulability. Section **3** presents the modeling of the human joint torque characteristics through a set of experiments involving human subjects. In addition, the effectiveness of the HFM is examined by using sets of simulated and empirical data on the maximum isometric force exerted by the human hand. Finally, Section **4** argues the close relationship between the OC and HFM in a manual shifting task by a subject's arm, and indicates that HFM can be used for evaluating/predicting the OC level from a limb's posture.

2 Human Force Manipulability Measure

The mechanism of a human limb is often modeled as a serial-link robotic manipulator using a set of n rotational joints. Its configuration (the limb's posture) can be represented with a vector composed of joint angles $\theta = (\theta_1, \theta_2, \cdots, \theta_n)^T \in \Re^n$. The relationship between the joint torque $\tau \in \Re^n$ and the force exerted by the endpoint $f \in \Re^m$ in the m-dimensional task space can then be given as follows:

$$\tau = J(\theta)^T f, \tag{1}$$

where $J(\theta) \in \Re^{m \times n}$ is the Jacobian matrix of the endpoint position $x \in \Re^m$ with respect to θ.

The force manipulability ellipsoid (FME) for robotic mechanisms [6] is defined as a pre-image of the unit sphere in the joint space $||\tau|| \leq 1$ and can be determined using Eq. (1), as follows:

$$\begin{aligned} ||\tau|| &= \tau^T\tau = (J^T f)^T (J^T f) \\ &= f^T J J^T f \leq 1. \end{aligned} \tag{2}$$

The FME shape indicates the performance index of the force generation ability in the direction of operation for a given posture θ. A large operational force can be exerted easily along the major axis of the FME, but it is difficult to do so along the minor axis. Although this fact has been widely used as a quantitative measure for evaluating the force generation ability at the endpoint for multi-body robotic mechanisms, it cannot provide a feasible result for the human extremities because no biological motor properties, such as torque limitation, the torque-angle relationship, and the viscoelastic properties of muscle, are considered.

Here, let $\alpha = (\alpha_1, \alpha_2, \cdots, \alpha_n)^T \in \Re^n$ $(0 \leq \alpha_i \leq 1)$ be a vector of the joint torque activation level. The element α_i represents the activation ratio of the i-th joint's torque τ_i to its maximum torque τ_i^{max} under the maximum voluntary contraction (MVC). Given that muscle tension is nearly proportional to the muscle activation level, τ can be rewritten with α, as follows:

$$\tau = T(\theta)\alpha, \tag{3}$$

where $T(\theta) = \mathrm{diag.}(\tau_1^{max}(\theta_1), \tau_2^{max}(\theta_2), \cdots, \tau_n^{max}(\theta_n))^T \in \Re^{n \times n}$ represents the matrix of the relationship between the maximum joint-torque and the joint-angle for human limb joints.

Substituting Eq. (1) into Eq. (3) yields

$$\alpha = T^{-1} J^T f. \tag{4}$$

The unit sphere in the muscle-activation space $||\alpha|| \leq 1$ makes an HFM ellipsoid (HFME), as follows:

$$\begin{aligned} ||\alpha|| &= \alpha^T\alpha = (T^{-1}J^T f)^T (T^{-1}J^T f) \\ &= f^T (T^{-1}J^T)^T (T^{-1}J^T) f \\ &= f^T (JT^{-1})(JT^{-1})^T f \leq 1. \end{aligned} \tag{5}$$

Equation (5) represents the fact that the HFME is scaled from the FME with the matrix $T(\theta)$, which reflects the human joint torque characteristics for a given joint angle. It is expected that, unlike FME, HFME can provide a rough estimate of the feasible magnitude of the force generated at the endpoint according to the limb posture, in addition to the geometrical features.

The spatial characteristics of HFME, such as shape, orientation, and size, can be obtained using the singular value decomposition (SVD) of JT^{-1}, as follows:

$$JT^{-1} = U_b \Sigma_b V_b^T, \tag{6}$$

where $U_b = [u_{b1}, u_{b2}, \cdots, u_{bm}] \in \Re^{m \times m}$ and $V_b = [v_{b1}, v_{b2}, \cdots, v_{bn}] \in \Re^{n \times n}$ are orthogonal matrices, $\Sigma_b = [\, \Sigma_{b0} \mid 0 \,] \in \Re^{m \times n}$, $\Sigma_{b0} = \mathrm{diag.}(\sigma_{b1}, \sigma_{b2}, \cdots, \sigma_{bm}) \in \Re^{m \times m}$ contains the non-zero singular values of JT^{-1} in decreasing order $(\sigma_{b1} \geq \sigma_{b2} \geq \cdots \geq \sigma_{bm} \geq 0)$. The principal axes of the HFME are derived as $u_{b1}/\sigma_{b1}, u_{b2}/\sigma_{b2}, \cdots, u_{bm}/\sigma_{bm}$ so that the HFME's shape and orientation can be calculated. The volume of the ellipsoid V_{bf} can also be obtained, as follows:

$$V_{bf} = \frac{c_m}{\sigma_{b1}\sigma_{b2}\cdots\sigma_{bm}} \tag{7}$$

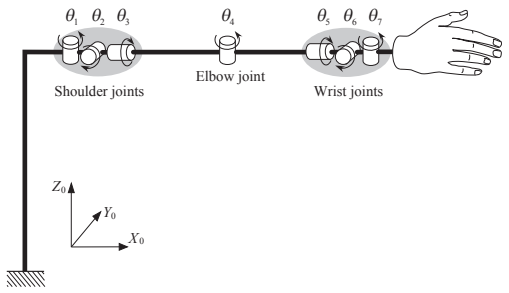

Fig. 1. Link model of human upper extremity with seven rotational joints.

where

$$c_m = \begin{cases} (2\pi)^{\frac{m}{2}}/2 \cdot 4 \cdot 6 \cdot (m-2) \cdot m & (m : even) \\ 2(2\pi)^{\frac{(m-1)}{2}}/1 \cdot 3 \cdot 5 \cdot (m-2) \cdot m & (m : odd). \end{cases}$$

3 HFM ANALYSIS OF HUMAN UPPER EXTREMITY

Considering the redundancy of an actual human arm, the arm is modeled as a multi-joint mechanism with three rigid links and seven degrees of freedom, as shown in Fig. 1. The arrows indicate the positive rotational direction, and the standard posture is defined in the figure. The agonists for uniarticular movements within the arm model were defined and are listed in Table 1.

3.1 Joint-torque Characteristics

Four healthy volunteers (Japanese male university students, aged 22 to 24) participated in the measurement test to model human joint-torque characteristics. The subjects' physical attributes are summarized in Table 2. The measurement tests were carried out with the subjects after briefly explaining the experimental procedure to them.

Fig. 2(a) shows an overview of the apparatus used to investigate the torque-angle relationship for a human arm joint, which consists of units for measuring the joint torque and EMG signals, and a biofeedback display for monitoring the muscle activation level during the experiments. A dynamometer (Biodex System 2AP, Medical Systems Inc., USA.) is used for measuring the isometric torque generated by uniarticular movements in the right upper extremity. Attachments were assembled according to the target joint movements, as shown in Fig. 2(b). Because of the Biodex system's mechanical structure, horizontal extension/flexion in the shoulder (θ_1) was replaced with extension/flexion, assuming the same agonist for the two uniarticular movements.

EMG signals were measured from the agonist for uniarticular motion using a set of disposable electrodes (Biorode SDC-H, GE Marquette Medical Systems, Japan) with an amplifier (MT11, NEC Medical Systems, Japan), and recorded using a personal computer linked via an analog/digital converter (sampling frequency: 1 kHz). The recorded EMG signal was rectified and integrated with data from the previous 0.1 s and normalized with the value in the MVC, premeasured at the neutral angle of the joint. The normalized value was used as the muscle contraction level in this study.

The subjects were instructed to monitor the biofeedback display and to generate an isometric torque with a uniarticular motion at the specified joint angle under a 40% muscle contraction level for 10 s. The joint angle was changed by 20 ° around the midpoint of the excursion, where the limit angle was used when the specified angle was greater than that of the excursion. Two sets of measurement tests were performed for each uniarticular movement. The data measured for each uniarticular movement was processed according to the following procedure:

1. Divide the measured temporal data into each second for each trial.
2. Calculate the average and standard deviation of the muscle contraction level in every period.
3. Extract, from all 20 periods, those 10 periods in which the average value is closest to the 40% muscle contraction level.
4. Calculate the average and standard deviation of the isometric joint torque for the 10 extracted periods.

TABLE 1
Agonist for each uniarticular movement.

Joint			Motion	Agonist
Shoulder	θ_1	+	Extension	Latissimus dorsi
		−	Flexion	Deltoideus anterior
	θ_2	+	Adduction	Pectoralis major
		−	Abduction	Deltoideus middle
	θ_3	+	Internal rotation	Teres major
		−	External rotation	Infraspinatus
Elbow	θ_4	+	Flexion	Biceps brachii
		−	Extension	Triceps brachii
Wrist	θ_5	+	Supination	Biceps brachii
		−	Pronation	Pronator teres
	θ_6	+	Ulnar deviation	Extensor carpi ulnaris
		−	Radial deviation	Flexor carpi radialis
	θ_7	+	Flexion	Flexor carpi radialis
		−	Extension	Extensor carpi ulnaris

TABLE 2
Physical attributes of subjects participating in isometric joint torque measurement test.

Subject	A	B	C	D
Age	23	22	22	22
Height [cm]	167	183	177	182
Weight [kg]	63	63	65	76

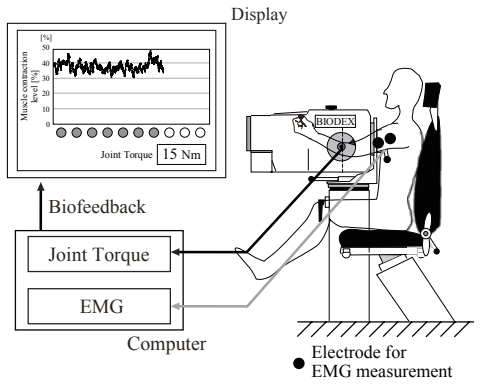

(a)

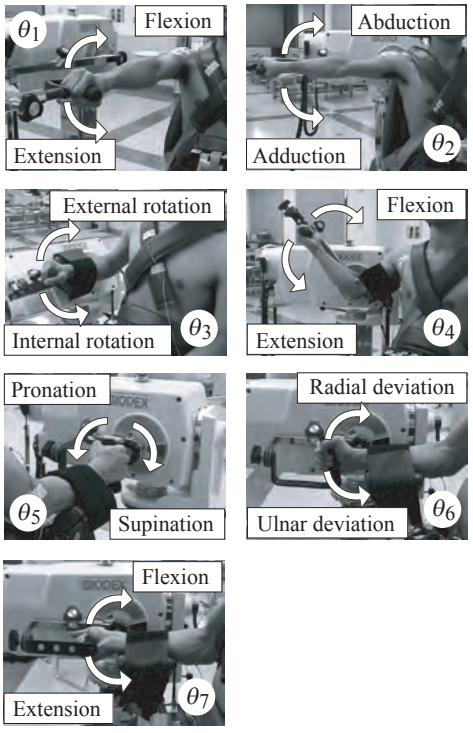

(b)

Fig. 2. Apparatus for measuring isometric joint torque caused by uniarticular motion. (a) Overview of original joint torque and EMG signal measurement system. (b) Photos of attachments for each joint of the upper extremity.

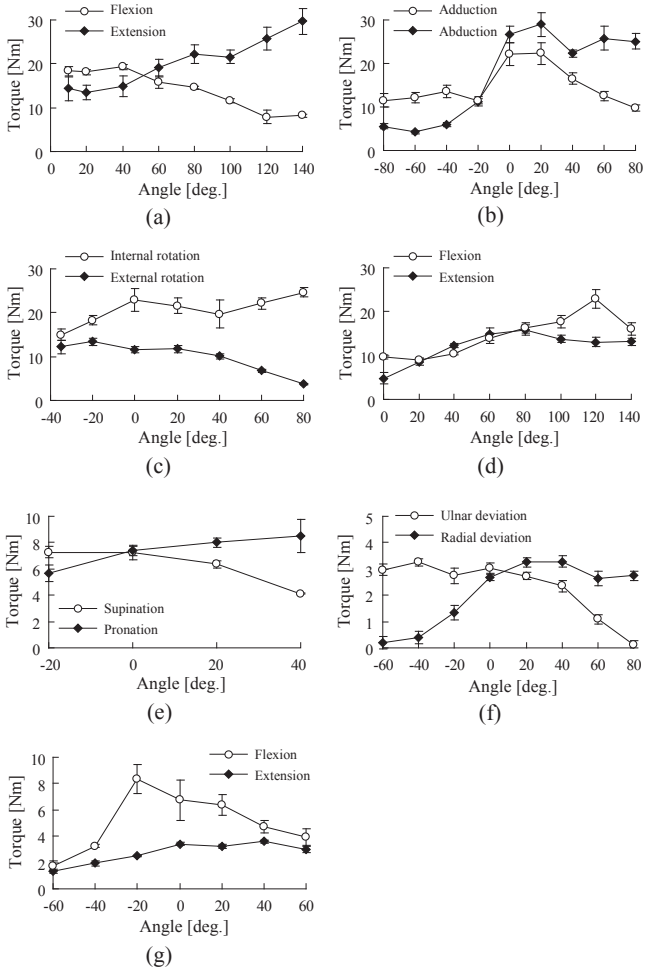

Fig. 3. Typical results for magnitude of isometric torques measured at 40% MVC for each uniarticular movement of the upper limb. The solid line with white circles represents the torque-angle relationship observed during uniarticular motion in the positive rotational direction, whereas the dotted line with black circles represents that in the negative rotational direction. (a) First joint of upper limb. (b) Second joint. (c) Third joint. (d) Fourth joint. (e) Fifth joint. (f) Sixth joint. (g) Seventh joint.

Fig. 3 presents a set of measured isometric joint torques with respect to the joint angle and direction of rotation for all seven joints, in which the vertical axis is the magnitude of the joint torque. The joint torque characteristics showed two tendencies in uniarticular movements; these tendencies support the biological evidence reported in the literature [12], [13], [14], [15], [16], [17]. The first tendency is that the joint torque is almost proportional to the joint angle, as is evident from the wrist radial deviation and ulnar deviation, as well as from the wrist pronation and supination. The second is that the joint torque peaks around the intermediate joint excursion angle, as shown in the elbow extension and wrist flexion. The same experimental results were found for all subjects, although some individual differences were found to exist. The mean values of the measured data for all the subjects are listed in Table 3.

The maximum isometric torque in each uniarticular motion was calculated by magnifying the measured value by 2.5, assuming that the joint torque generated by the uniarticular motion was almost linear relative to the agonist's muscle activation level. This was modeled using a fourth-order polynomial equation as a function of the joint angle, as follows:

$$\tau_i^{max}(\theta_i) = a_{4i}\theta_i^4 + a_{3i}\theta_i^3 + a_{2i}\theta_i^2 + a_{1i}\theta_i + a_{0i}. \quad (8)$$

TABLE 3
Means of isometric torque for all subjects.

θ_1 [deg.]		5#	10#	20	40	60	80	100	120	140
Torque [Nm]	+	20.89	15.09	17.98	17.80	18.54	18.19	17.00	14.36	12.56
		19.56	17.89	17.42	22.72	27.89	29.64	27.47	33.26	32.77
θ_2 [deg.]		-80	-60	-40	-20	0	20	40	60	80
Torque [Nm]	+	13.56	13.68	15.90	18.05	28.01	24.76	21.90	18.43	18.33
		6.42	5.83	6.58	9.82	17.45	19.98	18.18	18.79	21.28
θ_3 [deg.]		-40	-20	0	20	40	60	80		
Torque [Nm]	+	12.37	15.05	17.20	17.42	15.12	14.05	15.50		
		14.03	15.45	16.35	18.49	16.07	13.78	13.02		
θ_4 [deg.]		0	20	40	60	80	100	120	140	
Torque [Nm]	+	12.10	12.85	14.39	17.27	20.54	17.93	17.23	10.60	
		6.23	8.80	11.83	14.11	15.57	13.82	12.34	11.82	
θ_5 [deg.]		-60	-40	-20	0	20	40	60	80	
Torque [Nm]	+	0.33	0.91	1.36	1.80	1.97	2.08	2.33	2.27	
		3.62	3.40	3.63	3.50	3.00	1.32	0.87	0.29	
θ_6 [deg.]		-20	0	20	40					
Torque [Nm]	+	7.22	6.70	5.44	4.28					
		3.47	4.18	5.49	6.42					
θ_7 [deg.]		-60	-40	-20	0	20	40	60	80#	
Torque [Nm]	+	1.97	2.25	3.13	4.14	4.23	4.01	3.39	2.42	
		1.28	2.16	3.74	3.43	3.92	3.68	3.17	2.06	

Two of the four subjects

TABLE 4
Physical attributes of all subjects participating in measurement of operation forces while applying maximum effort.

Subject	1	2	3	4
Age	22	24	22	23
Height [cm]	174	166	172	174
Weight [kg]	64	60	65	70

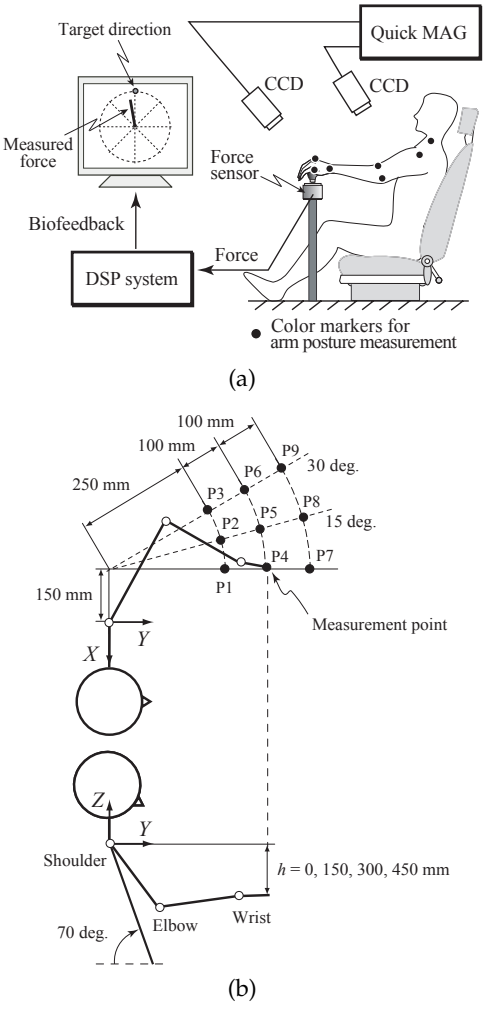

Fig. 4. Apparatus for HFM verification. (a) Overview of the original measurement system of operation force and arm posture for generating the maximum force. (b) Top and side views of the experimental condition at the specified measurement points.

The coefficients $a_{0i}, \cdots$, and a_{4i} were estimated using the least squares method. Based on the experimental evidence that a particular joint torque is almost proportional to the body weight [23], [24], the torque model's value was adjusted according to the weight of each subject in computing the HFMEs.

3.2 Spatial Characteristics of HFME and Human Operation Force

The validity of HFME was investigated through comparison with the maximum operation force exerted by the other four subjects (Japanese male university students, aged 22 to 24). The subjects' physical data is summarized in Table 4.

Fig. 4 shows the apparatus used for measuring the operation force and arm posture. As shown in Fig. 4(a), a knob and six-axis force/torque sensors are attached to the top of a rigid stick. The positions of multiple color markers attached to the measurement points on the body are recorded with a 3D motion capture system (Quick MAG, Ouyou Keisoku Kenkyusyo Inc., Japan), which can detect the three-dimensional position of a marker through the application of the provided software to a pair of two-dimensional image sequences captured with two CCD cameras in real time. The joint angles of the arm model are computed from the positional data of the markers while offline. The biofeedback display presents the target direction and the measured operation force vector while online. Fig. 4(b) shows the experimental conditions with consideration given to the arrangement of a shift lever in a general vehicle, where the black dots represent the measurement points. The arm posture was recorded at all points corresponding to four different heights h = 0, 150, 300, and 450 mm. The maximum operation force applied by the arm was measured at five points (P2, P4, P5, P6, and P8) for h = 150 mm and at three points (P2, P4, and P5) for h = 450 mm, based on the upper-lower range for gear-shifting operations in a general vehicle as well as the range of arm reaching.

The subjects were seated in front of the display, as

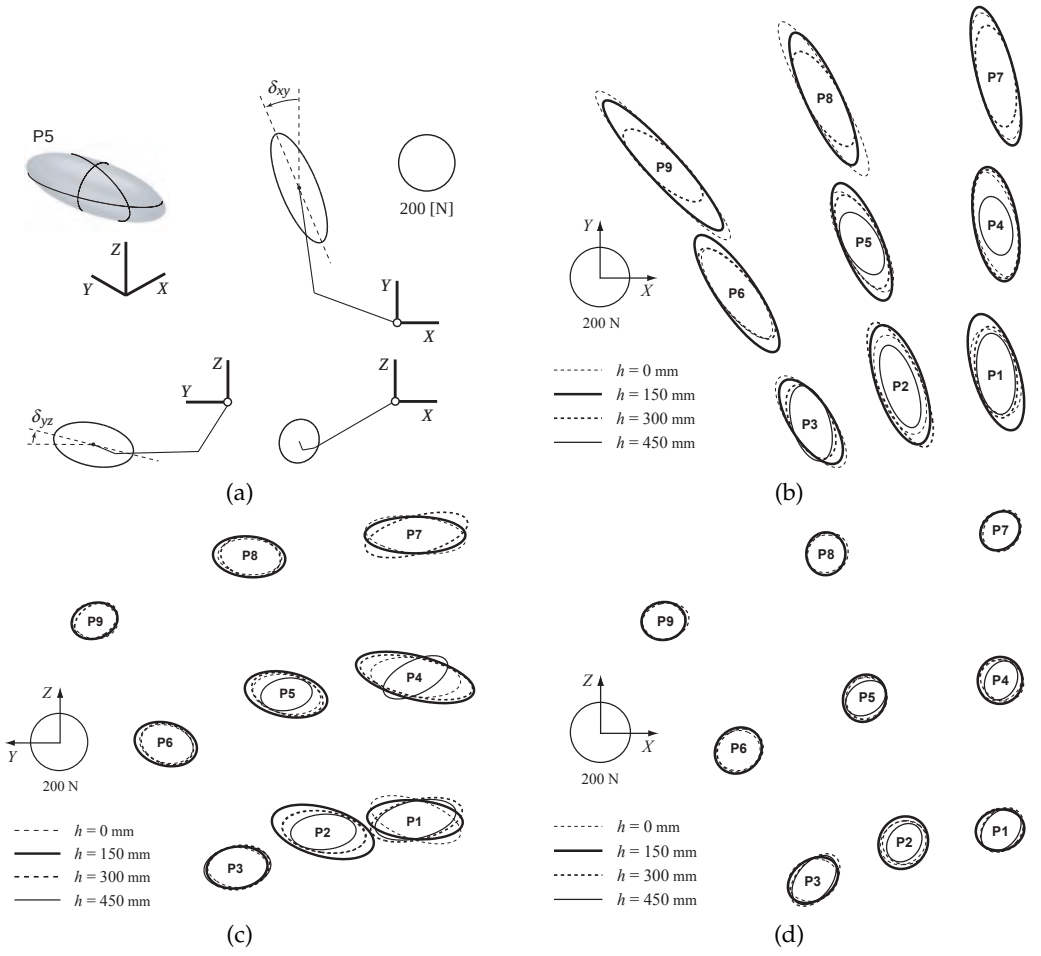

Fig. 5. Results of HFMEs for Sub. 1, calculated from the arm postures according to the specified measurement points in the horizontal plane at heights h = 0, 150, 300, and 450 mm. (a) HFM ellipsoid for the arm posture measured at P5. (b) HFMEs projected onto the X-Y planes. (c) HFMEs projected onto the Y-Z planes. (d) HFMEs projected onto the X-Z planes.

shown in Fig. 4(a). Their shoulders were held into the seat with a seatbelt. The subjects grasped the knob with their non-dominant (left) hand and determined the desirable arm posture for exerting larger forces in all specified directions. In the measurement of maximum operation force, they were instructed to exert the maximum effort to generate a larger operation force in the specified target direction in the horizontal plane (θ_d = 0, 45, $\cdots$, 315 °) for 5 s, while maintaining their arm postures.

The joint angles were calculated using the mean of the marker position data obtained with the arm model. The mean value of the 1-s measured data was considered to be the maximum operation force that could be applied by the arm, in which the variation of operation forces generated for 1 s was the smallest within the last 3 s.

Fig. 5 shows a set of HFMEs calculated from the arm postures for Sub. 1, measured at the specified measurement points in the four horizontal planes. The ellipse at each point denotes the cross-section of the HFME in the 2D plane as shown in Fig. 5(a). The size of the HFMEs on the X-Y (horizontal) plane becomes smaller as the hand position descends from the position of the shoulder joint (see Fig. 5(b)). In addition, the shape becomes more elliptical as the hand position moves forward from the body. Meanwhile, the orientation rotates counterclockwise as the hand position moves away and to the left. The size in the Y-Z plane becomes smaller as the hand position moves away and to the left of the body. The shape becomes rounder as the hand position moves away and to the left (see Fig. 5(c)). No notable distinctions can be seen in the Z-X plane under the experimental conditions of this study (see Fig. 5(d)).

Fig. 6 summarizes the spatial characteristics of the HFMEs for all of the subjects according to the height of the measurement points in the X-Y and Y-Z planes, such as the size (S), orientation (δ), and shape (β). The size in the 2D plane was calculated by singular values of JT^{-1}, as defined by Eq. (6), the orientation is the relative angle between the major

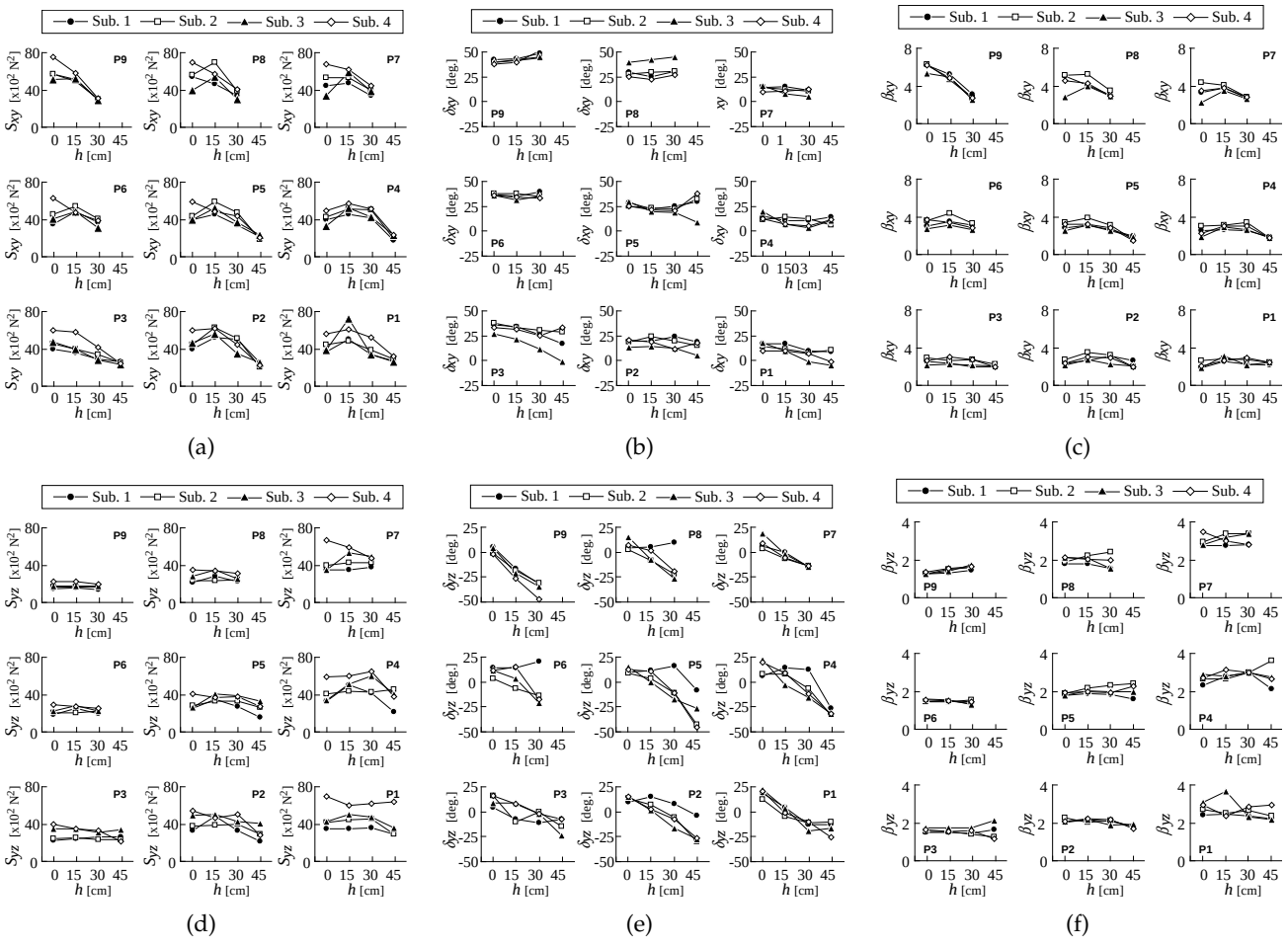

Fig. 6. Spatial characteristics of HFMEs depending on the height of the measurement points for all subjects. (a) Size of HFMEs on X-Y. (b) Orientation of HFMEs on X-Y. (c) Shape of HFMEs on X-Y. (d) Size of HFMEs on Y-Z. (e) Orientation of HFMEs on Y-Z. (f) Shape of HFMEs on Y-Z.

principal axis of the HFME and the X axis (see Fig. 5(a)), and the shape is the ratio of the norm of the major axis to that of the minor axis. The very similar properties depending on the height and position of the measurement point can be confirmed in the results for all of the subjects although slight individual differences can be observed. The indices S_{xy} and δ_{yz} change mainly with the height of the measurement points and β_{yz} mainly with the position; the others are affected by both factors.

Fig. 7 shows the measured forces generated by the subjects when exerting their maximum efforts in eight different directions in the X-Y planes with h = 150 and 450 mm, in addition to the HFMEs calculated from the arm postures. The black dots represent the measured data while the distance to the center of the HFME at each point denotes the magnitude of the measured operation force. The dots exist around the arc of the HFME at each point, and the magnitude of the maximum force changes according to the direction and hand positions in much the same way as the measured results reported by Nijhof and Gabriel [25], although some differences can be seen, especially in the major direction of HFME.

Fig. 8 shows the estimated error in the operation forces for each of two heights for all of the subjects, where each error is normalized with the maximum measured operation force. The center line in each box is the median, while the edges of the box correspond to 25% and 75%, respectively, with the whiskers extending to the most extreme data points, eliminating any outliers (plus sign). Most of the outliers correspond to the errors in the major direction of HFME. The magnitude of the calculated forces with HFMEs tends to become larger than the measured forces produced by the subjects, but the worst median value is less than about 0.3.

The aforementioned simulation and measurement results demonstrate that the proposed HFME can be utilized to analyze the spatial characteristics of the operation force exerted by a human hand with a maintained arm posture and can roughly estimate the production capability of the maximum operation force exerted by the arm in a certain direction.

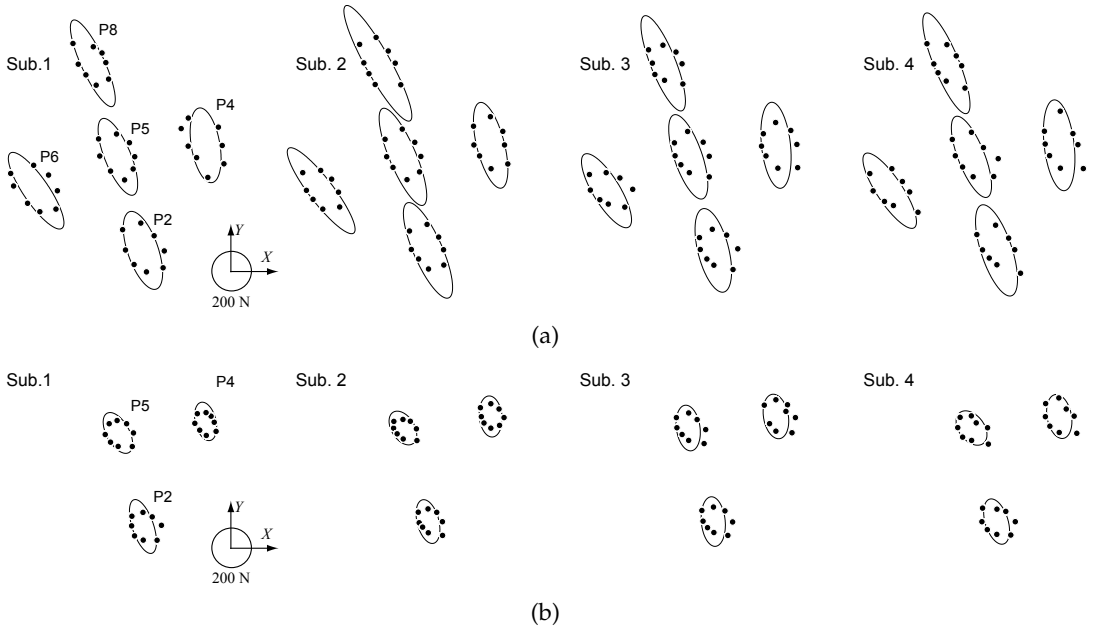

Fig. 7. Maximum operation forces exerted by subjects providing maximum effort and HFME at specified measurement points. The black dots and solid lines indicate the measured force and HFME, respectively. (a) Measured and simulated results at a height of h = 150 mm. (b) Measured and simulated results at a height of h = 450 mm.

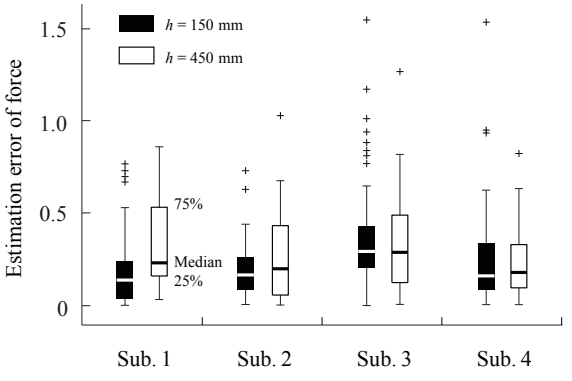

Fig. 8. Estimation error in forces normalized with the measured forces for all subjects.

4 OC Evaluation in Manual Shifting with HFM Measure

This section analyzes the relationship between the OC levels and HFME spatial characteristics during gear shifting and discusses why the OC depends on the arrangement of the shifter knob and arm posture by using HFME properties.

4.1 Apparatus and Method

Five healthy volunteers (Japanese male university students, aged 22 to 24) participated in a test for measuring OC when using an electric gear shifter, where the four volunteers (Subs. 1, 2, 3, and 4) participated in the measurement of the maximum operational force. The physical characteristics of an additional volunteer (Sub. 5) were age 24, height 180 cm, and weight 73 kg. The experiments were carried out after briefly explaining the experimental procedure to the participants, including the gear shifter operation.

Fig. 9 shows a schematic view of the gear-shifting system developed for this study. The system consists of a direct-drive linear motor table (Nippon Thomson Co., Ltd., Japan; maximum force $\pm$150 N) and a digital-signal-processing (DSP) board (ds1103, dSPACE, Germany) that can provide stable control and high-quality data measurement at a 1-kHz sampling frequency. A shifter knob and a six-axis force/torque sensor (NITTA, Ltd., Japan; resolution: force x axis: 6.1 $\times 10^{-3}$ N, y axis: 6.1 $\times 10^{-3}$ N, z axis: 1.2 $\times 10^{-2}$ N; torque: 1.1 $\times 10^{-3}$ Nm) are attached to the moving part of the linear motor table to measure the operation force generated during shifting. The subject's hand position is measured using an encoder built into the motor table (encoder resolution: 2 μm). The subject's arm movements during shifting are observed using a stereo camera (Quick-MAG, OKK, Japan).

A variable impedance control method [19], [20], [21], [22] was applied to control the motor table's motion so as to provide a realistic feeling of shifting from a low gear to second gear. The dynamic properties of the gear-shifter change according to the shifter knob position y_s, and can be represented as follows:

$$M\ddot{y}_s + B(y_s)\dot{y}_s + K(y_s)(y_s - y_e) = f_y, \qquad (9)$$

where M denotes the shifter knob inertia; $B(y_s)$ and

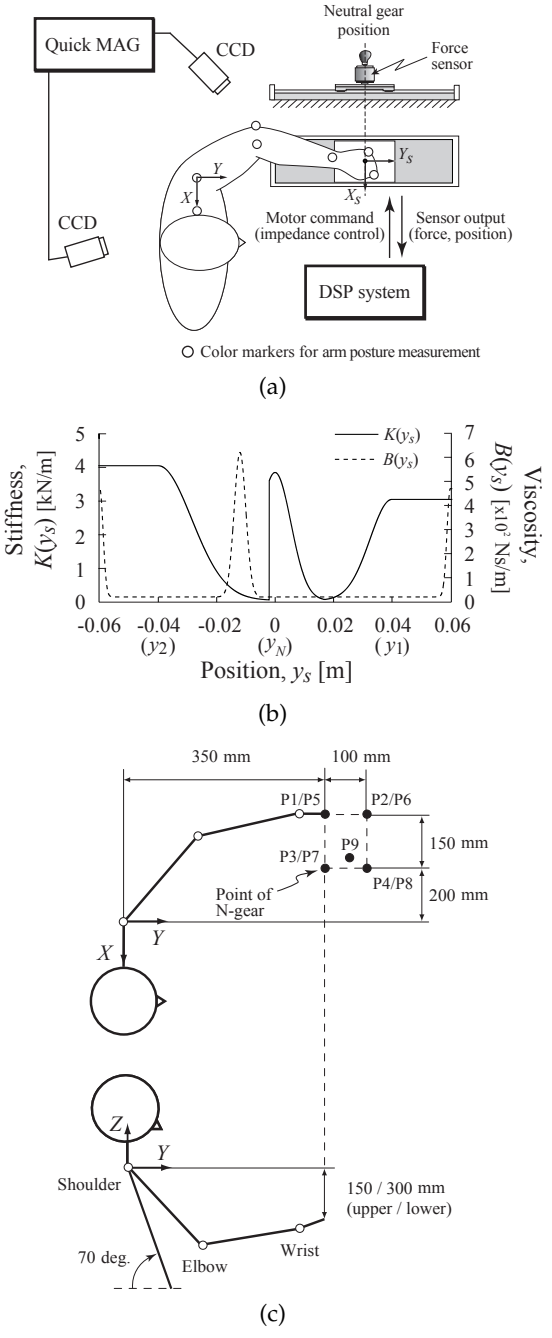

Fig. 9. Schematic diagram of developed electric gear-shifting system using robotic devices. (a) Overview of apparatus for measuring hand motion (position and force) and arm posture during manual gear shifting. (b) Designed viscoelastic pattern applied to the gear-shifting system. (c) Top and side views of the experimental condition at the nine specified points for the neutral gear.

$K(y_s)$ denote the variable viscosity and stiffness as a function of the knob's position y_s, respectively; y_e represents the equilibrium for $K(y_s)$ corresponding to the gear position; and f_y is the operation force along the Y_s axis exerted by the human operator.

TABLE 5
Best point for shifter knob for all subjects participating in gear-shifting test.

Subject		1	2	3	4	5
P9	X [mm]	-200	-200	-200	-200	-200
	Y [mm]	400	375	450	410	410
	Z [mm]	-300	-295	-200	-275	-300

The robot stiffness generates an artificial attraction force corresponding to the relative distance between the equilibrium y_e and the shifter knob's position y_s, while the robot viscosity provides an artificial viscous friction to the motion of the shifter knob. In the developed gear-shifting system, the equilibrium y_e is switched between the positions corresponding to the low gear y_1, neutral (N gear, hereafter) y_N, and second gear y_2, according to the shifter knob position y_s as:

$$y_e = \begin{cases} y_1 & (y_s > y_a) \\ y_N & (y_b \leq y_s \leq y_a) \\ y_2 & (y_s < y_b), \end{cases} \tag{10}$$

where y_a and y_b represent the switching points of the equilibriums. A viscoelastic pattern in each interval of these three gears can be designed with Gauss functions. Fig. 9(b) shows the viscoelastic pattern applied to the gear-shifting system, which was designed based on the force-to-stroke profile measured on an actual sedan-type vehicle. This was adjusted until a middle-aged male driver with excellent driving skills was satisfied with it after a series of shifting operation trials. The feeling of pulling the shifter out of each gear was enhanced by increasing the value of the stiffness around the equilibriums, and the subtle feeling of changing gear was well regulated by using the viscosity effect. The distance between the N gear and the other gears was set to 4 cm; i.e., y_1 = 4 cm, y_N = 0 cm, and y_2 = -4 cm, and the switching points at (y_a, y_b) = (1.7 cm , -0.2 cm). The shifter knob inertia M was set to 0.45 kg.

For the experiment, the subjects were seated parallel to the gear-shifting system, as shown in Fig. 9(a), and were asked to conduct three rounds of shifting operations between the low and second gears, while blindfolded, using their left hands. The gear-shifting operation tests were carried out at nine different points for the N gear (P1 $\sim$ P9), as shown in Fig. 9(c). The suitable point for each subject (P9), as determined in the preliminary tests, was the point at which the subject made the shift with the greatest degree of comfort within the target space containing the eight points. The details of P9 are summarized in Table 5. After each trial, they graded the OC as one of the following five levels: 5: "Very good," 4: "Good," 3: "Normal," 2: "Bad," and 1: "Very bad," relative to their memory of P9. Note that the point for the N gear was selected randomly from the specified nine points,

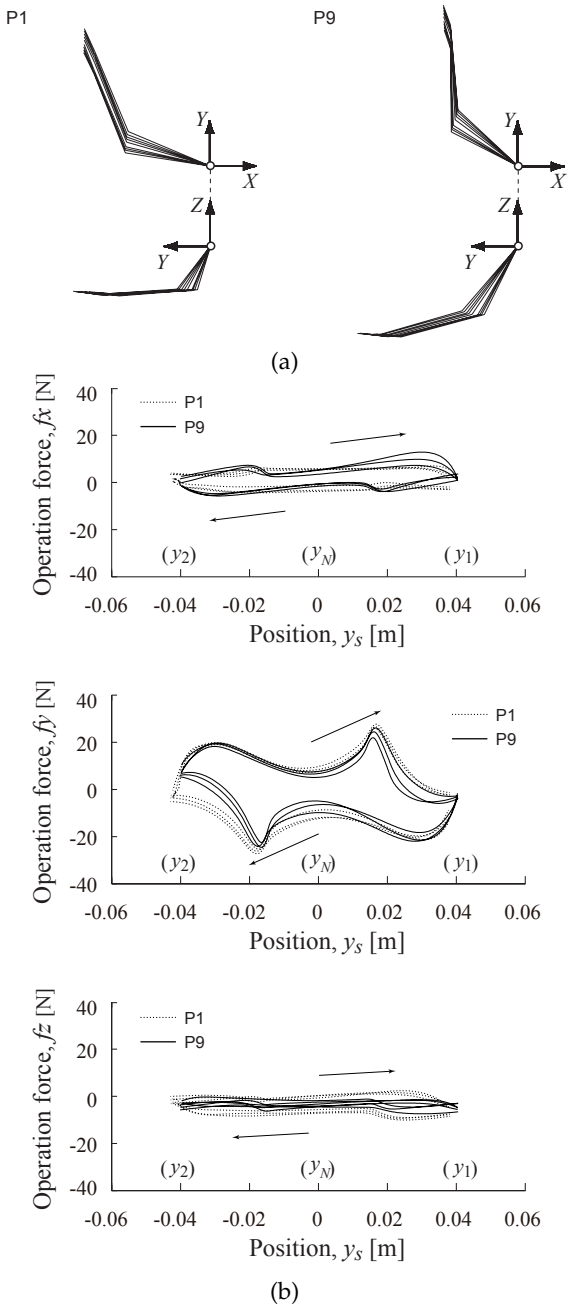

Fig. 10. Examples of measured results at points P1 and P9. (a) Stick pictures of the arm motion projected onto X-Y and Y-Z planes. (b) Hand motion profiles in the operation direction during shifting.

and three trials were performed for each point.

4.2 Relationship between HFME and OC

Fig. 10 represents typical measured results for the gear-shifting operations performed by a subject with his arm between the low and second gears at the two points P1 and P9. The arm postures recorded during the shifting were found to change depending on the arrangement of the shift lever (Fig. 10(a)), while the

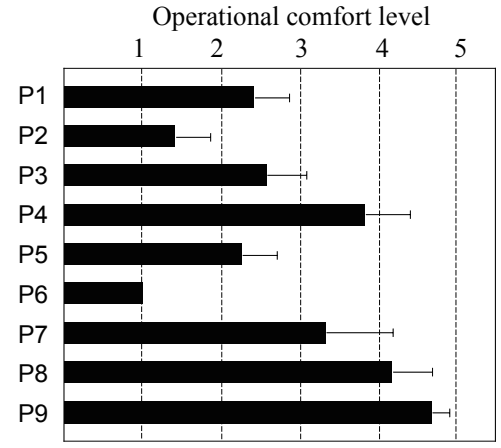

	P1	P2	P3	P4	P5	P6	P7	P8	P9
P1				**		**		**	**
P2			*	**			**	**	**
P3		*		**		**		**	**
P4	**	**	**		**	**			
P5				**		**	*	**	**
P6	**		**	**	**		**	**	**
P7		**			*	**			**
P8	**	**	**		**	**			
P9	**	**	**		**	**	**		

*: $p < 0.05$, **: $p < 0.01$

Fig. 11. Subjective evaluation results of OC for specified positions with multiple comparisons.

force-to-stroke profiles of the hand motion in the operational direction were almost the same (Fig. 10(b)). This indicates that the subject moved the shifter knob while producing an almost identical operation force irrespective of the specified point while regulating their arm configurations.

Fig. 11 presents the OC evaluation results, in which the mean value for all subjects is presented with the standard deviation for each point and the multiple comparison tests. As expected, the OC depends on the shifter knob location (the arm posture). The higher evaluations were given for those points around the ideal point P9 (i.e., P4, P7, and P8), whereas the lower evaluations were given for those points far from the subject's body (i.e., P1, P2, P3, P5, and P6). The lower evaluation for P3 reflects the fact that the subjects moved their arms unsteadily during the shifting because P3 was too close to their bodies, and the lowest evaluation for P6 resulted from the shifting operation being performed at the furthest point from the body.

Fig. 12 shows examples of the force vectors and HFMEs projected onto the X-Y and Y-Z planes for points P1 and P9, where the thick line represents the force vector for shifting from the low to the second gear and the thin line represents the corresponding reverse motion. Each of these vectors was calculated using the mean of the data measured within 5 mm

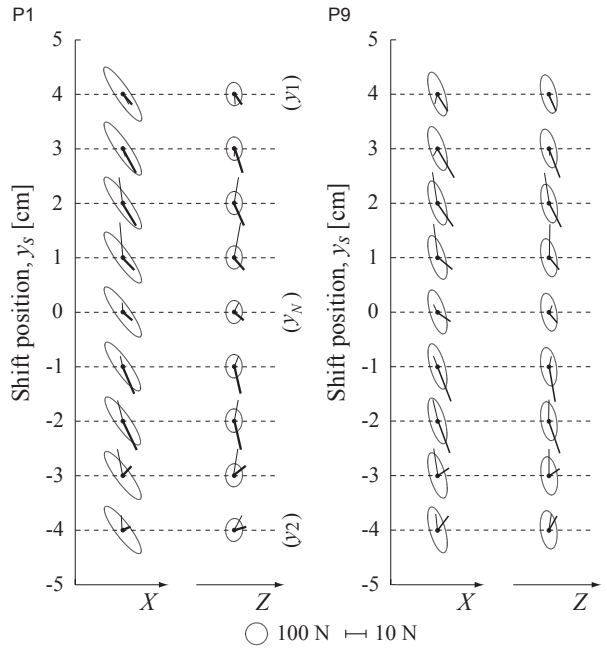

Fig. 12. Typical measured results for shifting operations at points P1 and P9. Spatial changes in force vectors and HFMEs projected onto X-Y and Y-Z planes.

TABLE 6
Relationship between OC and HFME.

		Subject 1	2	3	4	5
Orientation	δxy	**-0.783**	**-0.831**	**-0.698**	**-0.836**	**-0.924**
	δyz	0.331	0.501	0.243	0.329	0.535
Shape	βxy	-0.360	-0.236	-0.114	-0.460	-0.372
	βyz	**0.663**	**0.683**	**0.758**	**0.838**	**0.796**
Size	Sxy	0.089	0.095	0.254	-0.324	-0.005
	Syz	**0.713**	**0.845**	**0.760**	**0.729**	**0.665**

behind and in front of the black dot. Note that the operation forces applied by the hand during the shifting motion were unaffected by the shifting position because the subjects repeated stable arm motions during shifting (Fig. 10(b)). On the other hand, the spatial characteristics of the HFMEs are different at the two locations of the shifter knob. The orientation of the HFMEs in the X-Y plane for P9 tends to agree with the direction of movement (the y-axis), and the size of P9 in the Y-Z plane is much larger than that for P1. Very similar tendencies were found in the results for the other subjects. Table 6 summarizes the correlation coefficients between the geometric characteristics of the HFMEs in the X-Y and Y-Z planes and the OC levels at the nine points for each of the five subjects. The OC is closely correlated to δ_{xy}, β_{yz}, and S_{yz}, although there were some individual differences. These results suggest that the OC level was improved

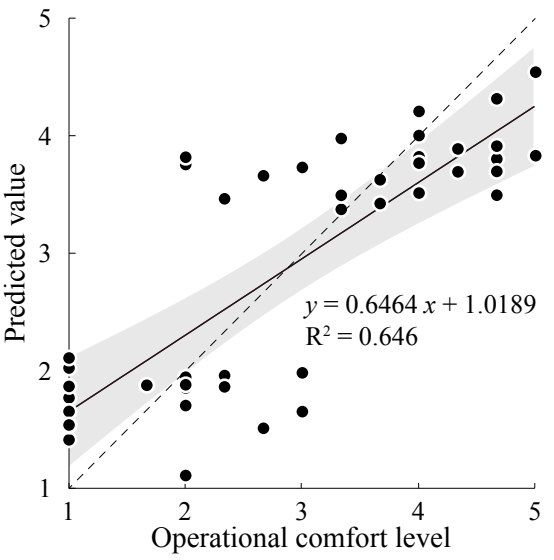

Fig. 13. Relationship between OC levels and predicted values using multiple regression model.

at those points at which the HFMEs in the X-Y plane were directed along the direction of shifting, whereas the HFMEs in the Y-Z plane were larger and became sharper in the direction of shifting. Consequently, we can say that there is a close relationship between the OC and the HFM measure for the force generation performance.

Based on the above-mentioned results for the data for all the subjects, the relationship between the OC and the spatial characteristics of HFME was analyzed using a multiple regression model as

$$Y = a_0 + \Sigma_{i=1}^{3} a_i X i, \tag{11}$$

where the dependent value Y is the OC level and the three independent values $X1$, $X2$, and $X3$ are δ_{xy}, β_{yz}, and S_{yz}, respectively. The estimated coefficients were $a_0 = 4.951$ ($p = 0.001$), $a_1 = -0.101$ ($p = 0.0004$), $a_2 = -0.032$ ($p = 0.94$), and $a_4 = 0.071$ ($p = 0.774$), respectively, and R-squared was 0.646. The smallest p-value for δ_{xy} indicates that the OC level is most affected by the relative angle of the HFME's major axis from the direction of shifting by the arm. This explains why the subjects could easily operate the shifter knob at that point at which they could exert a sufficiently large operation force in the direction of shifting. Fig. 13 shows the prediction results obtained with the multiple regression model, in which the regression line shows the relationship between the OC levels and predicted values, and the shading represents the 95% confidence region. Although a lower level of modeling reliability is observed around the middle OC level, the proposed HFME can be used not only for analyzing the spatial characteristics of motor performance in the hand space for a given arm posture but also for predicting the OC level during shifting operations. Future work will involve adding data for other

subjects while investigating the influence of verbal categories utilized in the OC evaluation.

5 Discussion and Conclusions

This paper has proposed a human force manipulability (HFM) measure, including human joint torque-angle characteristics, for calculating the spatial characteristics of the ability of a human to generate a force at the end-point of a limb, and has discussed a method based on HFM for evaluating/predicting the OC level during manual tasks performed by that limb. The usefulness of the proposed method for OC evaluation was verified through a set of experiments on gear shifting with an upper extremity.

First, the HFM was formulated by introducing human joint torque characteristics into robot force manipulability. An HFM verification test was then carried out via two experiments: 1) Isometric measurement of the joint torque characteristics for each of the seven upper limb joints, and 2) measurement of the maximum operation forces generated by the non-dominant hand with maintained arm postures. The measured data for the joint torque-angle showed that the magnitude of the isometric joint torques changed according to the joint angle and rotational direction within the range of motion of the joints. The HFMEs for the arm postures were then calculated and analyzed using the measured joint torque characteristics data, and the results demonstrated that the forces calculated from the HFMEs represented the major characteristics of the measured maximum force data in the two horizontal planes. This supports the measured results that indicated that the maximum isometric operation force in the horizontal plane depends on the direction [25]. In addition, the HFME can calculate the force production performance with a feasible magnitude for the specified limb's posture along a certain direction in the task space, but not limited to the horizontal plane.

Next, an operational arm-based test was performed by using the developed gear-shifting system. The results illustrated the influence of the shifting arrangement on the OC levels and the arm postures, while the human subjects operated the gear-shifter with almost the same operation force for all of the specified N-gear points. This supports the finding that the moment of a certain joint contributes to the making of a decision regarding comfort/discomfort during motion tasks [2], [4]. It would be valuable to compare the OC levels ranked by the five verbal categories with those ranked by the nine verbal categories that are often utilized in studies that rate the level of comfort/discomfort, but this is relatively unimportant to the discussion of the results of this study.

Finally, the relationship between the OC level and the geometrical properties of the HFME during gear shifting was determined. A statistical analysis showed that human operators felt more comfortable at those points where the HFME size in the vertical plane in the operating direction was larger and when the orientation of the HFME major axis was directed in the operational direction in the horizontal plane. The results indicate that the human OC level of interface devices can be predicted/evaluated by utilizing the HFMEs for various arm postures. Since the proposed method using the HFM can simulate the activation level of all of the joints involved in the motion by calculating backwards with Eq. (1), we could further investigate the contribution of the joints' activations on the OC levels during manual tasks by a limb.

This study used a small number of subjects for each experiment, but this will not influence the proposed methodology using HFM. From the application viewpoint, the database of human joint torque properties should be enriched to ensure the reliability of the proposed methodology while considering the individual effects, such as the gender, age [17], weight [23], [24], and joint combinations in the joint torque production [16], [18] as well as in the OC evaluation [3].

In conclusion, this study has focused on gear shifting with an upper extremity, but lower extremities could also be studied to the same ends. Future research will investigate the influence of the muscle contraction level on the joint torque characteristics so as to improve the reliability of the HFME and for expanding its application to other studies in terms of effort [26], [27], force [28], [29], [30], as well as the analysis of human movement in the operation of other human-machine systems.

Acknowledgment

The authors would like to thank Dr. T. Nouzawa with Mazda Motor Corporation for his contributions to the progress of this research and the reviewers for their helpful comments and suggestions that have greatly improved the manuscript.

References

[1] D. Kee and W. Karwowski: "Ranking systems for evaluation of joint and joint motion stressfulness based on perceived discomforts," *Applied Ergonomics*, Vol. 34, pp. 167–176, 2003.

[2] X. Wang, B.L. Breton-Gadegbeku, and L. Bouzon: "Biomechanical evaluation of the comfort of automobile clutch pedal operation," *national Journal of Industrial Ergonomics*, Vol. 34, pp. 209–221, 2004.

[3] P. Mukhopadhyay, L. O'Sullivan, and T.J. Gallwey: "Estimating upper limb discomfort level due to intermittent isometric pronation torque with various combinations of elbow angles, forearm rotation angles, force and frequency with upper arm at 90° abduction," *International Journal of Industrial Ergonomics*, Vol. 37, pp. 313–325, 2007.

[4] D. Kee and I. Lee: "Relationships between subjective and objective measures in assessing postural stresses," *Applied Ergonomics*, Vol. 43, pp. 277–282, 2012.

[5] H. Asada: "Geometrical representation of manipulator dynamics and its application to arm design," *Transaction of the ASME, Journal of Dynamic Systems, Measurement, and Control*, Vol. 105, pp. 105–135, 1983.

[6] T. Yoshikawa: "Analysis and control of robot manipulators with redundancy," *Robotic Research: the 1st International Symposium*, eds. M. Brady and R. Paul. MIT Press, Cambridge, Mass., pp. 735–747, 1984.
[7] P. Chiacchio, Y. B.-Vercelli, and F. Pierrot: "Force polytope and force ellipsoid for redundant manipulators," *Journal of Robotic Systems*, Vol. 14, No. 8, pp. 613–620, 1997.
[8] T. Yoshikawa: "Dynamic manipulability of robotic mechanisms," *Journal of Robotic Systems*, Vol. 2, No. 1, pp. 113–124, 1985.
[9] K. Ohta, M. M. Svinin, Z. W. Luo, S. Hosoe, and R. Laboissière: "Optimal trajectory formation of constrained human arm reaching movements," *Biological Cybernetics*, Vol. 91, pp. 23–36, 2004.
[10] A. Otsuka, T. Tsuji, O. Fukuda, M. E. Shimizu, and M. Sakawa: "Development of an internally powered functional prosthetic hand with a voluntary closing system and thumb flexion and radial abduction," Proceedings of *the 2000 IEEE International Workshop on Robot and Human Interactive Communication*, pp. 405-410, 2000.
[11] M. Hada, Y. Amano, K. Fukui, and S. Doi: "An evaluation of vehicle steering arrangement with dexterity measures of virtual human," *SAE Technical Paper (Digital Human Modeling for Design and Engineering Conference)*, 2001-01-2109, 2001.
[12] N. Salter, and H. D. Darcus: "The effect of the degree of elbow flexion on the maximum torques developed in pronation and supination of the right hand," *Journal of Anatomy*, Vol. 86, pp. 197–202, 1952.
[13] J. S. Leedham, and J. J. Dowling: "Force-length, torque-angle and EMG-joint angle relationships of the human in vivo biceps brachii," *European Journal of Applied Physiology*, Vol. 70, pp. 421–426, 1995.
[14] T. Uchiyama, T. Bessho, and K. Akazawa: "Static torque-angle relation of human elbow joint estimated with artificial network technique," *Journal of Biomechanics*, Vol. 31, pp. 545–554, 1998.
[15] M. A. Welsch, P. A. Williams, M. L. Pollock, J. E. Graves, D. N. Foster, and M. N. Fulton: "Quantification of full-range-of-motion unilateral and bilateral knee flexion and extension torque ratios," *Academy of Physical Medicine and Rehabilitation*, Vol. 79, pp. 971–978, 1998.
[16] F. Guenzkofer, H. Bubb, V. Senner, and K. Bengler: "Dependency of knee extension torque on different types of stabilization," *International Journal of Human Factors Modelling and Simulation*, Vol. 3, No. 1, pp. 1-15, 2012.
[17] S. Hisamoto, M. Higuchi, and N. Miura: "Age-related differences of extremity joint torque of healthy Japanese," *Journal of Gerontechnology*, Vol. 4, No. 1, pp. 27–45, 2005.
[18] http://www.dhergo.org/
[19] N. Hogan: "Impedance control: An approach to manipulation: Parts I, II, III," *ASME Journal of Dynamic Systems, Measurement, and Control*, Vol. 107, No. 1, pp. 1–24, 1985.
[20] R. Ikeura and H. Inooka: "Variable impedance control of a robot for cooperation with a human," Proceedings of *the 1995 IEEE International Conference on Robotics and Automation*, pp. 3097–3102, 1995.
[21] T. Tsuji and Y. Tanaka: "Tracking control properties of human-robotic systems based on impedance control," *IEEE Transactions on Systems, Man, and Cybernetics-Part A: Systems and Humans*, Vol. 35, No. 4, pp. 523–535, 2005.
[22] Y. Tanaka, N Yamada, T. Tsuji and T. Suetomi: " Vehicle Active Steering Control System Based on Human Impedance Properties of the Arms," *IEEE Transactions on Intelligent Transportation Systems* , Vol. 15, No. 4, pp. 1758 - 1769, 2014.
[23] G. Markovic and S. Jaric: "Scaling of muscle power to body size: the effect of stretch-shortening cycle," *European Journal of Applied Physiology*, Vol. 95, pp. 11–19, 2005.
[24] S. Jaric and G. Markovic: "Normalizing physical performance tests for body size: A proposal for standardization," *Journal of Strength and Conditioning Research*, Vol. 19, No. 2, pp. 467–474, 2005.
[25] E. J. Nijhof and D. A. Gabriel: "Maximum isometric arm forces in the horizontal plane," *Journal of Biomechanics*, Vol. 39, No. 39, pp. 708–716, 2006.
[26] K. H. Kim, B. J Martin, and D. B. Chaffin: "Modelling of shoulder and torso perception of effort in manual transfer tasks," *Ergonomics*, Vol. 47, No. 9, pp. 927–944, 2004.
[27] C. R. Dickerson, B. J. Martin, and D. B. Chaffin: "Predictors of perceived effort in the shoulder during load transfer tasks," *Ergonomics*, Vol. 50, No. 7, pp. 1004–1016, 2007.
[28] S. C. Gandevia and D.I. McClosky: "Sensations of heaviness," *Brain*, Vol. 100, pp. 345–354, 1977.
[29] L. A. Jones: "Role of central and peripheral signals in force sensation during fatigue," *Experimental Neurology*, Vol. 81, pp. 497–503, 1983.
[30] R. G. Carson, S. Riek, and N. Shahbazpour: "Central and peripheral mediation of human force sensation following eccentric or concentric contractions," *Journal of Physiology*, Vol. 539, No. 3, pp. 913–925, 2002.

Yoshiyuki Tanaka received his B.E. degree in Computer Science and Systems Engineering from Yamaguchi University in 1995, and his M.E. and Dr. of Eng. degrees in Information Engineering from Hiroshima University in 1997 and 2001, respectively. He was a Research Associate with Hiroshima City University from 2001 to 2002, and an Assistant Professor with the Graduate School of Engineering at Hiroshima University from 2002 to 2013. He is currently an Associate Professor with the Graduate School of Engineering at Nagasaki University. His research interests include biological sensory-motor control mechanism and its application to human-machine systems. Dr. Tanaka is a member of the Japan Society of Mechanical Engineers, the Robotics Society of Japan, the Japan Ergonomics Society, the institute of Electrical Engineering of Japan, and the Society of Instrumentation and Control Engineers in Japan.

Kazuo Nishikawa received his B.E. degree in Mechanical Engineering from the University of Meiji in 1986. He was an Engineer of Craftsmanship development Gr. at Mazda Motor Corporation from 1986 and a Manager from 2002 to 2010. He is currently a General Research Manager of Technical Research Center at Mazda Motor Corporation from 2012. Mr. Nishikawa is a member of the Japan Society of Mechanical Engineers, the Society of Automotive Engineers of Japan, the Society of Instrumentation and Control Engineers in Japan, and Japan Ergonomics Society.

Naoki Yamada received his B.E. and M.E. degree in Mechanical Engineering from the University of Kyoto in 1990 and 1992, respectively. He was a Research Engineer of Technical Research Center at Mazda Motor Corporation from 1992 and an Assistant Manager from 2001. He is currently a Senior Specialist of Technical Research Center at Mazda Motor Corporation. His research interests include Kansei Engneering/Ergonomics of vehicle and development and application of human measurement and simulation device. Mr. Yamada is a member of the Japan Society of Mechanical Engineers, the Society of Automotive Engineers of Japan, the Japan Ergonomics Society.

Toshio Tsuji received his B.E. degree in industrial engineering in 1982, his M.E. and Dr. of Eng. degrees in systems engineering in 1985 and 1989, all from Hiroshima University. He was a Research Associate from 1985 to 1994, and an Associate Professor, from 1994 to 2002, in Faculty of Engineering at Hiroshima University. He was a Visiting Professor of University of Genova, Italy for one year from 1992 to 1993. He is currently a Professor with the Graduate School of Engineering at Hiroshima University. Dr. Tsuji won the K. S. Fu Memorial Best Transactions Paper Award of the IEEE RAS in 2003. His current research interests have focused on Human-Machine Interface, and computational neural sciences, in particular, biological motor control. Dr. Tsuji is a member of the Institute of Electrical and Electronics Engineers, the Japan Society of Mechanical Engineers, the Robotics Society of Japan, and the Society of Instrumentation and Control Engineers in Japan.